Myeloid cells from Langerhans cell histiocytosis patients exhibit increased vesicle trafficking and an altered secretome capable of activating NK cells

Daniel W. Hagey,[1,2] Egle Kvedaraite,[2-4+] Mira Akber,[3+] André Görgens,[1,5] Joman Javadi,[1] Tatiana von Bahr Greenwood,[2,6] Caroline Björklund,[7] Selma Olsson Åkefeldt,[2,8] Tova Hannegård-Hamrin,[9,10] Henrik Arnell,[11,12] Katalin Dobra,[1] Nikolas Herold,[2,6] Mattias Svensson,[3] Samir El Andaloussi,[1] Jan-Inge Henter[2,6] and Magda Lourda[2,3]

[1]Department of Laboratory Medicine, Karolinska Institutet, Stockholm, Sweden; [2]Childhood Cancer Research Unit, Department of Women's and Children's Health, Karolinska Institutet, Stockholm, Sweden; [3]Center for Infectious Medicine, Department of Medicine Huddinge, Karolinska Institutet, Karolinska University Hospital, Stockholm, Sweden; [4]Department of Clinical Pathology and Cancer Diagnostics, Karolinska University Hospital, Stockholm, Sweden; [5]Institute for Transfusion Medicine, University Hospital Essen, Essen, Germany; [6]Pediatric Oncology, Astrid Lindgren Children's Hospital, Karolinska University Hospital, Stockholm, Sweden; [7]Department of Pediatric Hematology and Oncology, Umeå University Hospital, Umeå, Sweden; [8]Theme of Children's Health, Karolinska University Hospital, Stockholm, Sweden; [9]Department of Physiology and Pharmacology, Karolinska Institutet, Stockholm, Sweden; [10]Department of Pediatric Anesthesia and Intensive Care, Karolinska University Hospital, Stockholm, Sweden; [11]Pediatric Gastroenterology, Hepatology and Nutrition, Astrid Lindgren Children's Hospital, Karolinska University Hospital, Stockholm, Sweden and [12]Department of Women's and Children's Health, Karolinska Institutet, Stockholm, Sweden

[+]EK and MA contributed equally to this work.

Correspondence: D. Hagey
daniel.hagey@ki.se

M. Lourda
magdalini.lourda@ki.se

Received: January 4, 2023.
Accepted: March 9, 2023.
Early view: March 16, 2023.

https://doi.org/10.3324/haematol.2022.282638

Supplemental information

Supplemental methods

Supplemental figures and legends

Supplemental references

Supplemental tables (provided separately as excel files)

Legends for supplemental tables:

Table S1: Characteristics of LCH patients included in the study.

Table S2: Count matrix (levels of gene expression) of samples from 3 controls and 3 LCH patients measured in triplicates (A-C). Neg: No INFγ treatment, pos: INFγ treatment.

Table S3: DESeq differential expression of all genes enriched in control and patient cells including the GO terms for the top 20 enriched genes.

Table S4: Count matrix (levels of gene expression) of samples from 5 pediatric controls (PC) and 3 pediatric patients with Crohn's disease (CD) measured in triplicates (A-C).

Table S5: Count matrix (levels of gene expression) of EVs from 5 controls and 4 LCH patients measured in triplicates (A-C).

Table S6: DESeq2 differential expression of all genes enriched in control and patient EVs including the GO terms for the top 20 enriched genes.

Table S7: DESeq2 differential expression of all genes enriched in EVs from patients with non-active or active disease including the GO terms for the top 20 enriched genes.

Table S8: Flow cytometry panel used in the study.

Supplemental methods

RNA sequencing (RNA-seq)

RNA from cells or EVs was extracted[1] and precipitated as previously described[2]: briefly, by incubating with 500µl TRI Reagent (Sigma-Aldrich, St. Louis, USA), adding 100µl chloroform and shaking vigorously. After 15 minutes at room temperature, samples were centrifuged at 12 000 x g for 15 minutes at 4°C and 300µl of the aqueous phase was added to 300µl isopropanol, 30µl of 3M sodium acetate and 1µl Pellet Paint (Merck, New Jersey, USA) before incubating over night at –20°C. Samples were then centrifuged at 20 000 x g for 30 minutes, pellets were washed twice in 600µl of 70% ethanol, dried and resuspended in 15µl elution buffer. RNA concentration was measured using the Qubit RNA High Sensitivity Assay (Thermo Fischer Scientific, South Logan, US) and 2ng were used as input to the Smart-seq2 protocol.[3] 50bp single end reads were sequenced on a HiSeq3000 (Illumina) and mapped to the ENSEMBL human transcriptome GRCh37 using Tophat 2.1.1 to generate the read count matrix, which was normalized using DESeq2.[4]

Principal component analysis (PCA), hierarchical clustering, differential gene expression, gene ontology analysis, batch correction and gene overlap enrichment

To gain an unbiased perspective, we pared the data down to the variable genes (as in Hagey *et al*[5]) in the data set expressed above 1 or 3 normalized counts for cells and EVs, respectively. PCA was executed using prcomp, while hierarchical clustering was performed on sample-to-sample Pearson correlations using hclust in R. Differential expression was calculated by the DESeq2 package to compare sample groups in R. Genes with an adjusted p-value below 0.01 or 0.05 for cells and EVs respectively, were separated into those that were upregulated or downregulated and analyzed using panther.org complete biological processes statistical overrepresentation test ontology database release 2019-12-09. A control group of all up- and

downregulated genes graphed together was calculated such that fold enrichments displayed for each individual group were divided by the enrichment in the control group. As we sequenced moDC samples from healthy pediatric controls and pediatric patients with Crohn's disease separately to our initial cohort, batch corrections were performed using ComBat in R.[6] Gene overlap enrichment was performed as: (# overlapping genes)/(# genes in group one)*(# genes in group two).[7] The mapping of GO terms to single cell data from Halbritter *et al*[8] was analyzed using Seurat pipeline V3[9] (https://satijalab.org/seurat/), was visualized using SeqGeq v1.6 from FlowJo (https://www.flowjo.com/solutions/seqgeq).

Luminex protein analysis

500µl of cell media was first concentrated to 50µl before analysis. A human premixed multi-analyte kit (R&D Systems) was then used to assess the levels of 10 selected factors secreted by DCs and/or monocytes according to the manufacturer's instructions, as in Javadi *et al.*[10]

Size exclusion chromatography, nanoparticle tracking and protein concentration measurement

500µl or 1ml of cell media from three LCH patients and three healthy controls ± INFγ treatment was run on qEVoriginal 70nm columns (Izon SP1) according to the manufacturer's instructions as previously described.[2] Briefly, columns were primed with 0.2µm filtered phosphate buffer saline (PBS) and samples were allowed to pass through the column before 10ml of PBS was applied on top. 3ml of PBS was first discarded before the four 1.5ml fractions were collected.

Nanoparticle tracking was performed on all size exclusion fractions using a Nanosight LM10 (Malvern Panalytical, UK) as previously described to calculate the concentration of particles.[10] Protein concentrations were calculated using a colorimetric DC protein assay (BioRad,

California, USA) according to manufacturer's instructions. Concentrations were back calculated to the original volume of media applied to size exclusion to get a per ml measurement of particle and protein concentrations.

Multiplex bead-based EV flow cytometry

For EV surface marker expression profiling, EVs were subjected to multiplex bead-based flow cytometry analysis (MACSPlex Exosome Kit, human, Miltenyi Biotec), as previously described.[11] In brief, equal volumes of EV containing samples were incubated with 8µl of MACSPlex Exosome Capture Beads (containing 39 different antibody-coated bead subsets). Captured EVs were counterstained with a mixture of APC-conjugated anti-CD9, anti-CD63 and anti-CD81 detection antibodies (supplied in the kit; 5µl each). Flow cytometric analysis was performed in a MACSQuant Analyzer 10 flow cytometer (Miltenyi Biotec). FlowJo software (v10, FlowJo LLC) was used to analyze raw flow cytometric data. Median fluorescence intensities (MFI) for each capture bead subset were background-corrected by subtracting respective MFI values from matched non-EV buffer or media controls that were treated exactly like EV-containing samples (buffer/medium + capture beads + antibodies).

Flow cytometry data analysis of lymphocytes

The cells were collected and stained as previously described[12] using a cocktail of the antibodies shown in Table S8. Data analysis was performed using FlowJo version 10 as described in Lourda *et al*.[13] Briefly, a compensation matrix was generated using AutoSpill, optimized and applied to all fcs files. All data was pre-processed with the time gate followed by exclusion of doublets, dead cells and lineage positive cells (CD14, CD15, CD19, CD304). 38000 lymphocytes from each individual were exported in a new file, barcoded and concatenated. Dimensionality reduction was performed with the Uniform manifold approximation and

projection (UMAP) FlowJo plugin v3.1. FlowJo Phenograph v3 was used for unsupervised clustering, with the optimal k-nearest neighbors (KNN) implemented automatically.

Transmission electron microscopy (EM) imaging

moDCs that had been cultured in the presence of INFγ (as described above) were pelleted after centrifugation for 5 min at 1500 rpm, followed by fixation in 2.5% glutaraldehyde in 0.1M PBS pH 7.3. The samples were then washed in 0.1M PBS and post-fixed in 2% osmium tetroxide in 0.1M PBS for 2 h at room temperature and embedded into LX-112 (Ladd, Burlington, Vermont, USA). Ultrathin sections (50-60 nm) were cut using a Leica ultracut UCT/Leica EM UC 6 (Leica, Wien, Austria). Sections were subsequently contrasted with uranyl acetate followed by lead citrate and examined in a Hitachi HT 7700 (Tokyo, Japan) microscope. Digital images were taken using a Veleta camera (Olympus Soft Imaging Solutions, GmbH, Münster, Germany).

For EV images, cell media was applied and stained with uranyl acetate as in Hagey *et al*[2] and imaged on a Tecnai 12 Spirit BioTwin microscope (FEI Company).

Lymphocyte stimulation assay

PBMC were isolated from buffy coats from 3 healthy donors and were resuspended in a concentration of 1 million cells/ml medium in the presence of anti-CD28 (0.34 µg/ml Thermo Fischer Scientific). The medium was either a mix of supernatants from 3 LCH cultures or a mix of supernatants from 3 control cultures. PBMC (200000 cells/well) were seeded in 6-well plates that had been coated with anti-CD3 monoclonal antibody (1µg/ml, Thermo Fischer Scientific) for 2h at 5% CO2 at 37°C, followed by aspiration and removal of the anti-CD3

solution before addition of the PBMC. The cells were left in culture for 18h before collection and staining for flow cytometry.

Supplemental figures

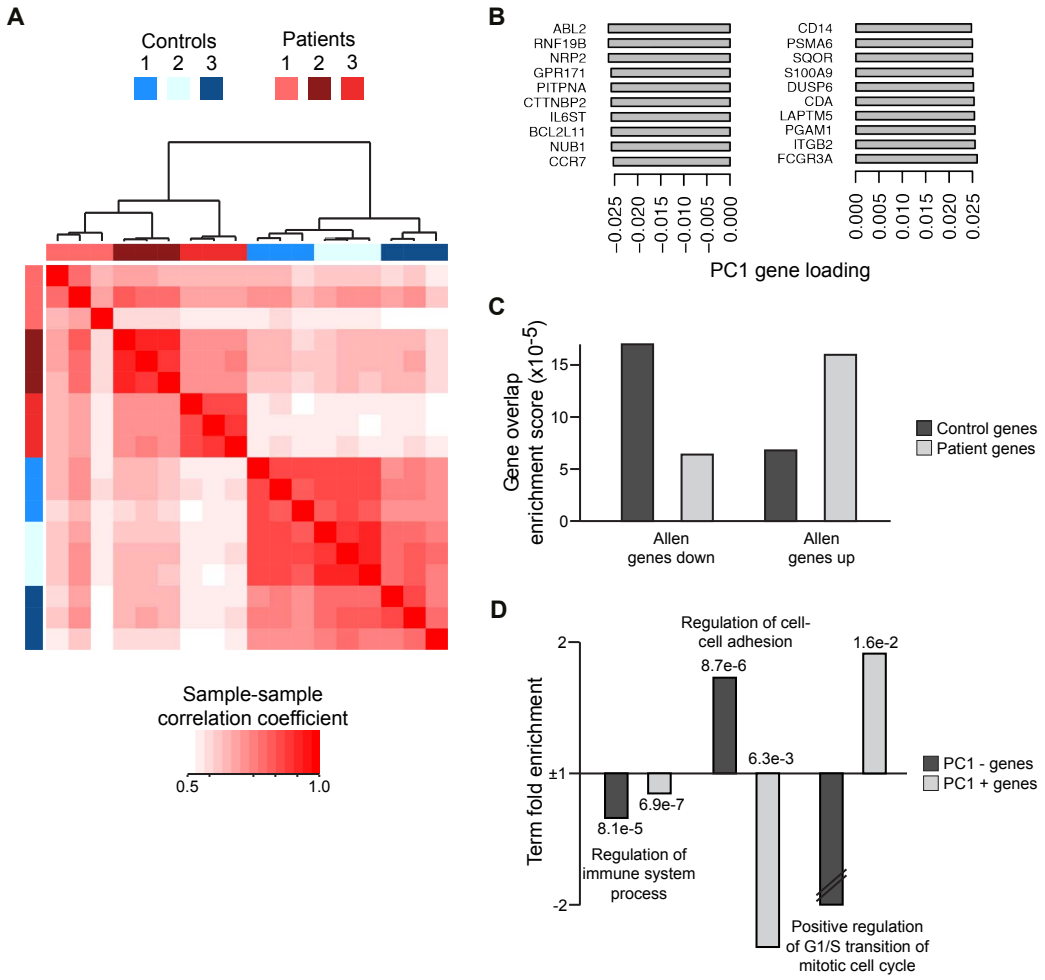

Figure S1. Variation in patient and control moDCs. (A) Hierarchical clustering of sample-sample Pearson correlations between control and patient moDCs. (B) Top principal component 1 loading genes for the principal component analysis (PCA) shown in **Figure 1E**. (C) Overlap enrichment of control and patient CD207^{+} cell enriched genes from Allen *et al*[14] and those differentially expressed in our control and patient moDC cells. (D) Gene ontology term fold enrichments for top 100 positively and negatively principal component 1 loaded genes for PCA shown in **Figure 1E**.

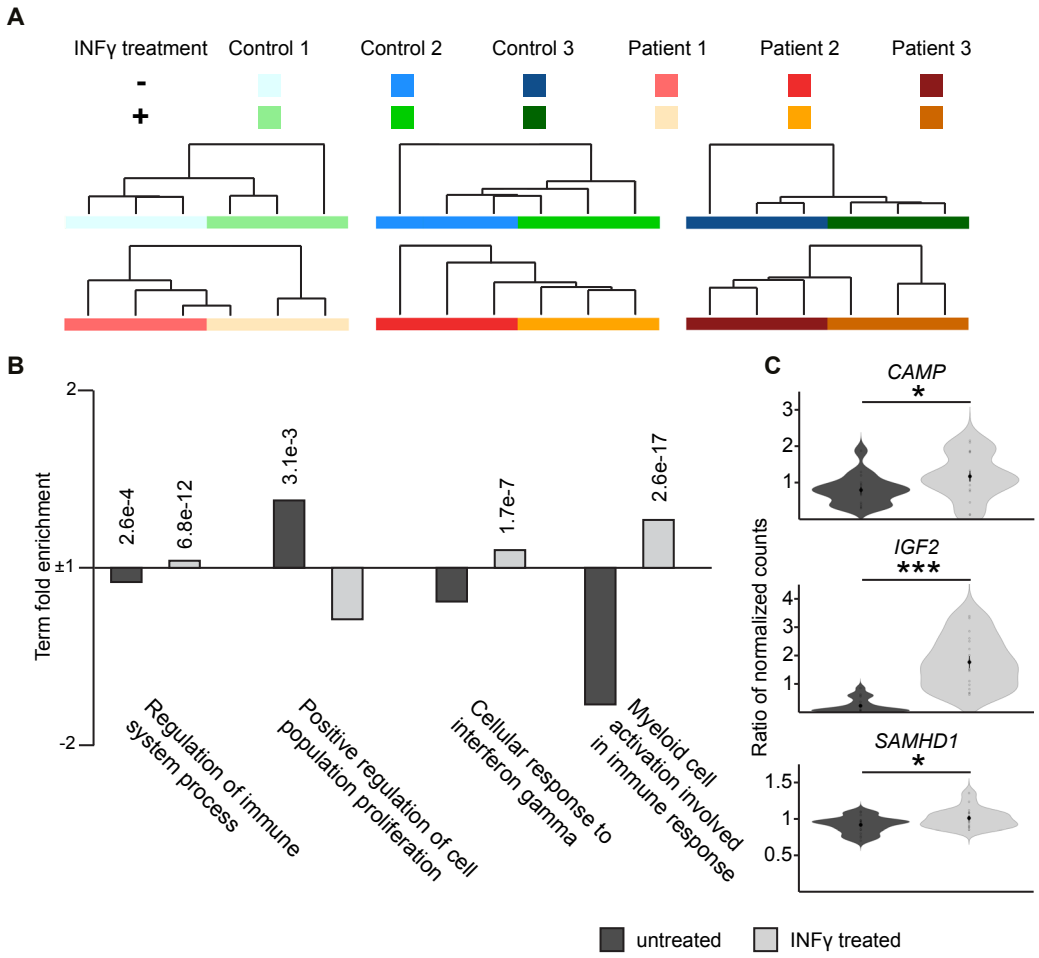

Figure S2. The effect of INFγ treatment on moDC maturation. (A) Hierarchical clustering of sample-sample Pearson correlations between INFγ treated and untreated moDCs from each individual control and patient. (B) Gene ontology term fold enrichments for all genes up and downregulated in moDCs by INFγ treatment. (C) Ratio of normalized count data in INFγ treated control and patient moDC for genes exemplifying the gene ontology pathways regulated in (B). Statistics performed using two-tailed, unpaired t-tests. * = $p<0.05$ and *** = $p<0.001$.

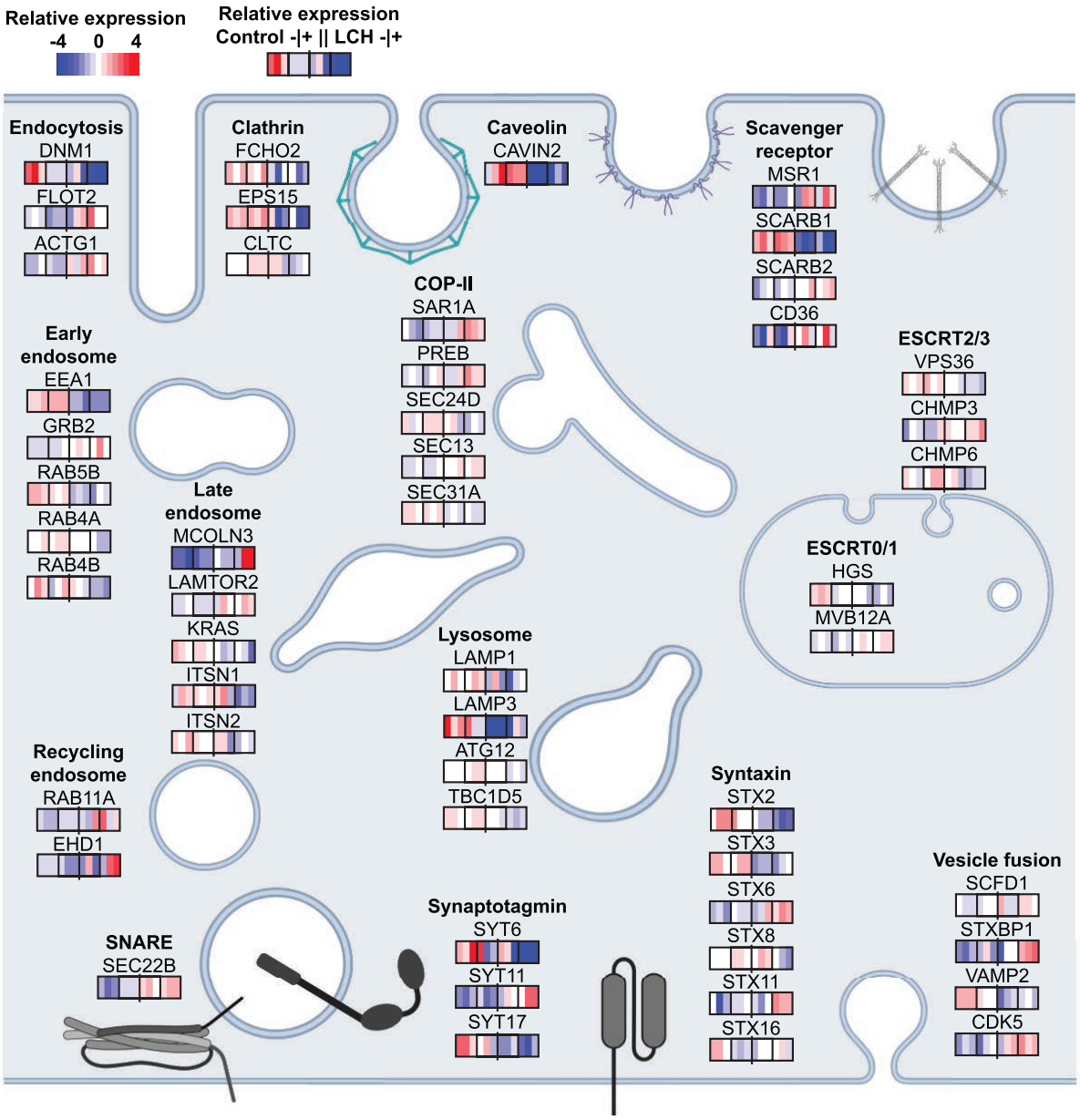

Figure S3. Dysregulation of multiple vesicle trafficking pathways. Heatmaps of relative normalized count data of selected important genes that are significantly different ($p<0.05$ using DESeq2) from various pathways involved in endocytosis, endosomal sorting and exocytosis in control and patient cells ± INFγ treatment. Individual triplicate values are displayed in the order: control INFγ- | control INFγ+ | patient INFγ- | patient INFγ+.

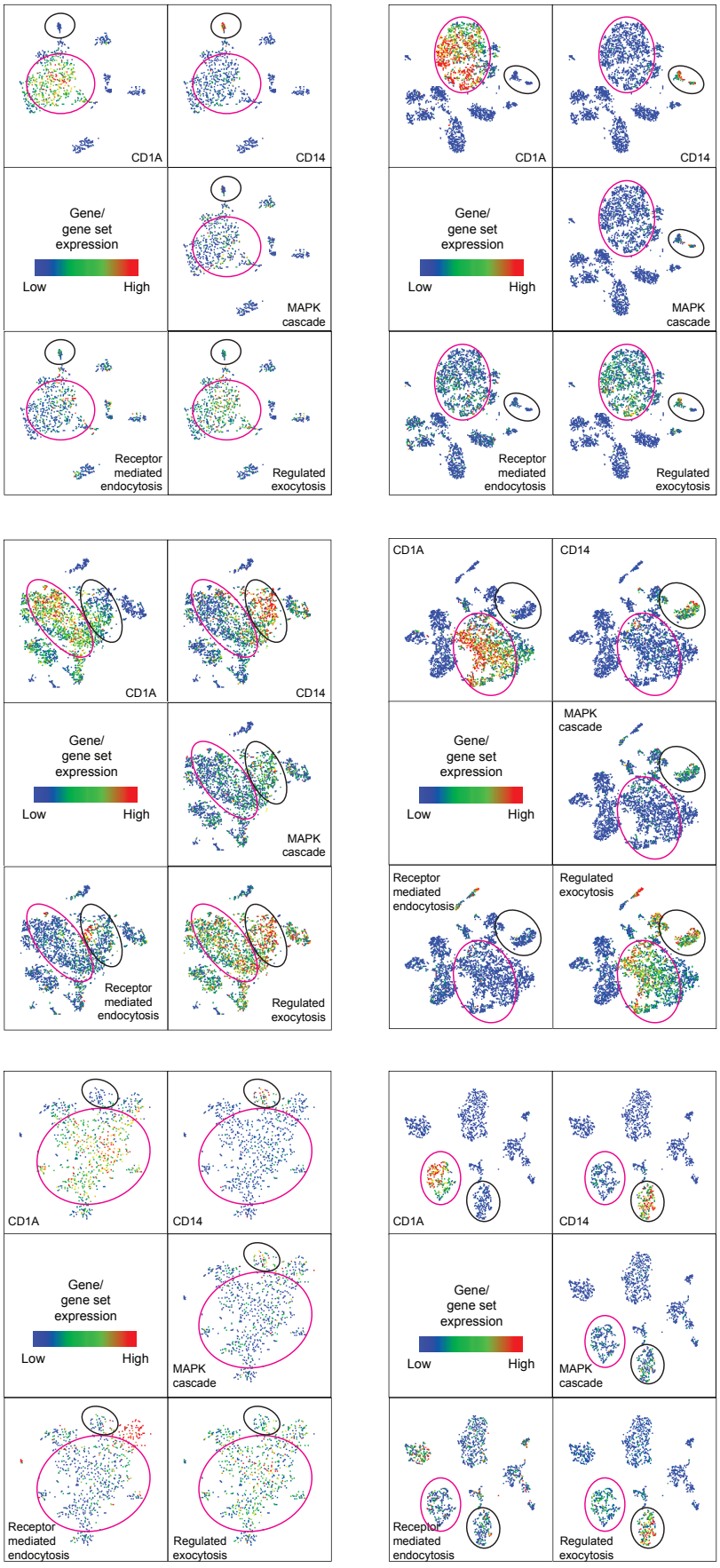

Figure S4. Mapping in lesional samples gene ontology terms that are enriched in patient moDC cultures. Single cell RNA-sequencing data from Halbritter *et al*[8] showing the expression of markers for LCH cells (*CD1A,* pink circle) and monocytes/ macrophages (*CD14,* black circle), as well as the genes that we found differentially expressed within the gene ontology terms listed in all patient lesions analyzed.

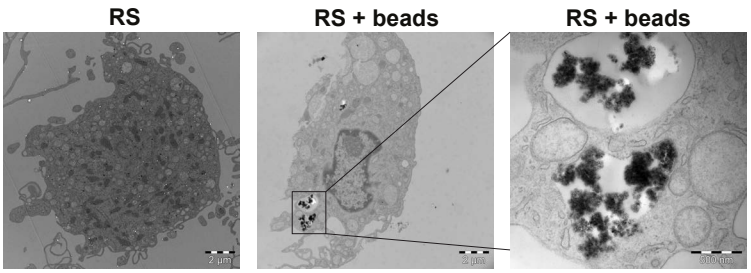

Figure S5. moDC endocytosis of beads. moDCs differentiated from monocytes that had been isolated with immunodensity negative selection (RosetteSep Human Monocyte Enrichment Cocktail, Stem Cell Technologies, RS). Isolation that does not include bead-based selection does not have any of the intracellular structures observed in **Figure 4**. Subsequent incubation of these moDCs for 2 hours with the beads used in the EasySep protocol (50 µl/ml) resulted in internalization of the beads (RS + beads).

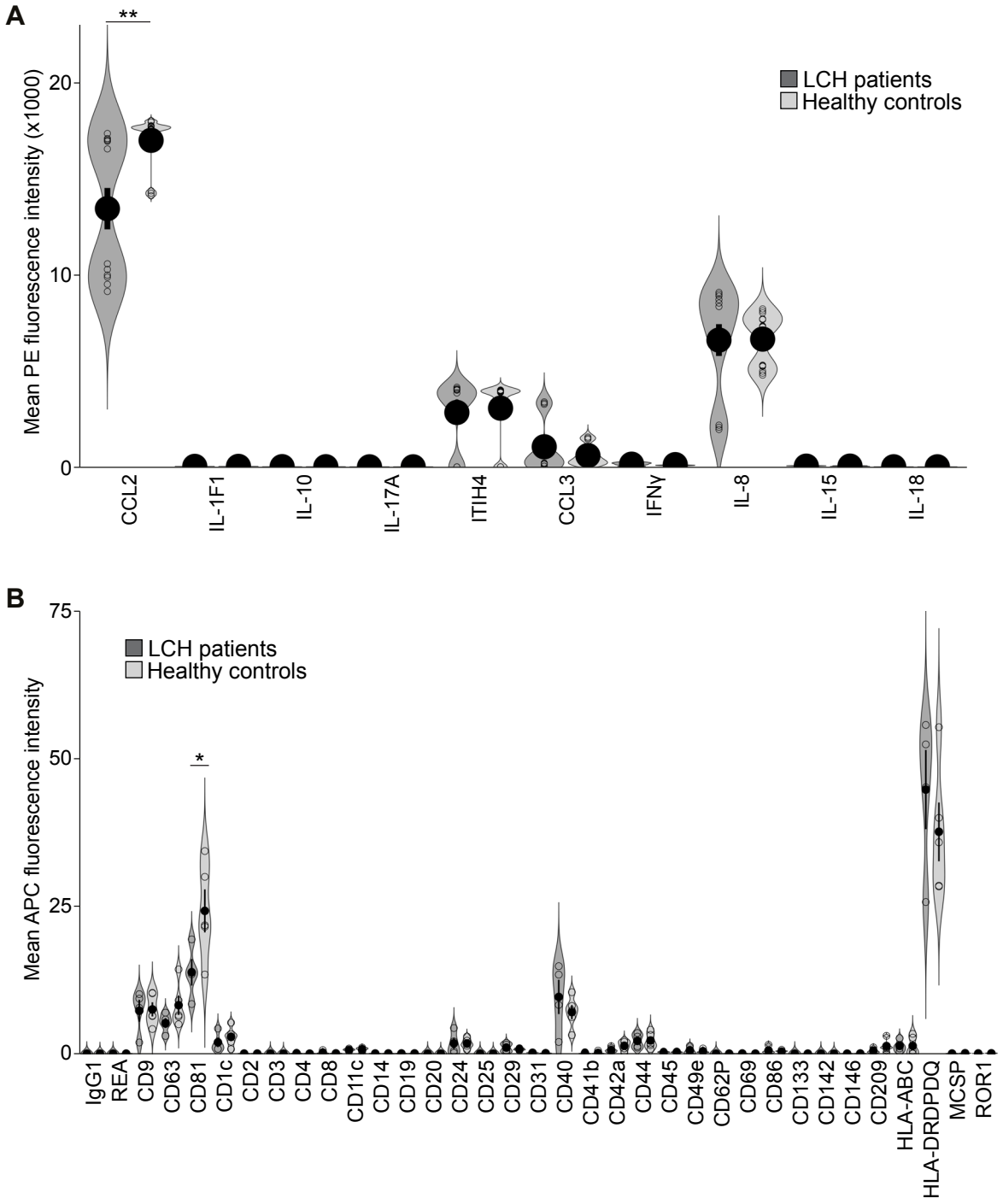

Figure S6. Multiplex analysis of moDC secretome proteins. (A) Luminex protein assay for cytokines known to be secreted by monocytes and DCs. (B) MACSplex EV surface protein flow cytometry assay for 39 standard proteins. Each maker in both assays corresponds to two sets of data points, with the left (dark grey) data points corresponding to patient and the right (light grey) data points to control samples.

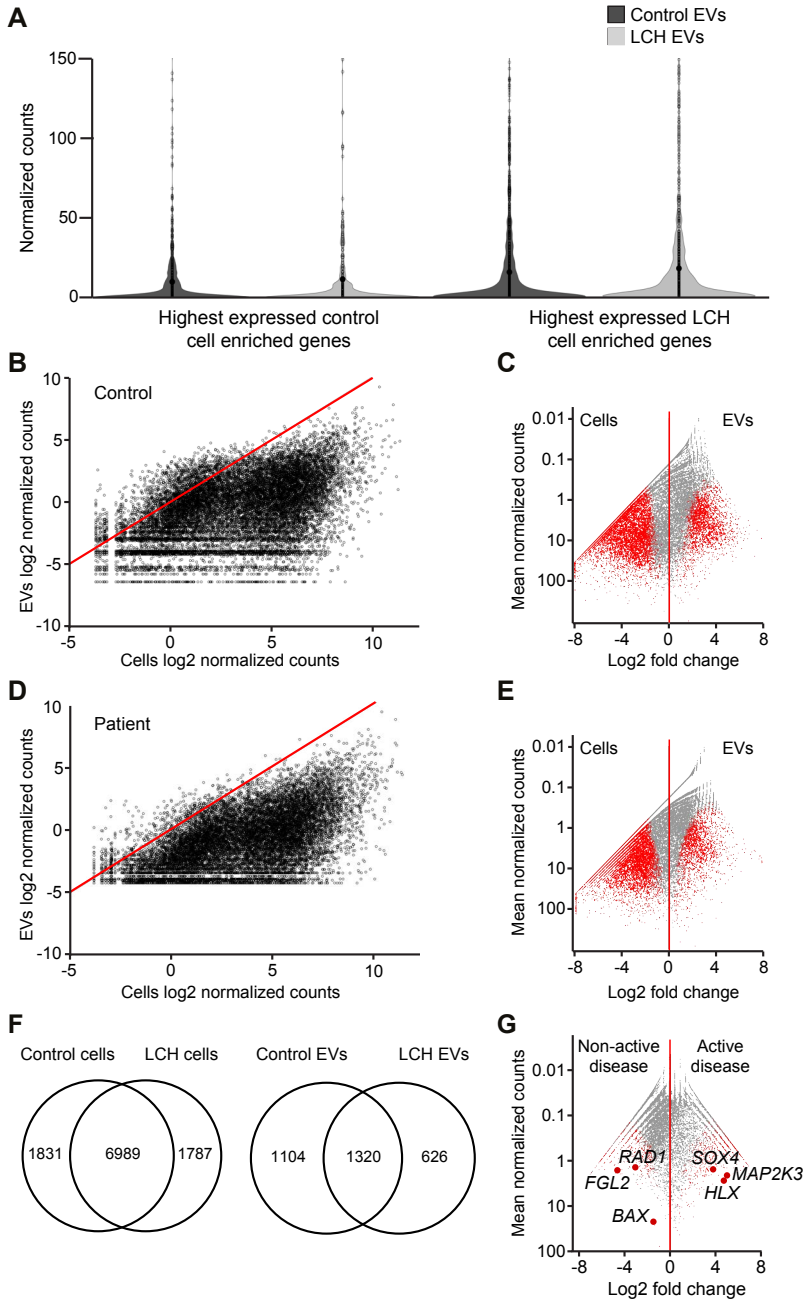

Figure S7. EV enriched transcripts are not the highest expressed genes in their cells of origin. (A) Patient and control EV normalized counts of the 100 genes with the greatest absolute difference in expression between patient and control cells. (B) Log2 normalized counts of genes in control moDC cells and EVs. Dots above red line are genes relatively more abundant in EVs than cells. (C) Gene expression comparison between control moDC cells and EVs. (D) Log2 normalized counts of genes in patient moDC cells and EVs. Dots above red line are genes relatively more abundant in EVs than cells. (E) Gene expression comparison between patient moDC cells and EVs. (F) Venn diagrams showing the overlap between genes enriched in control and patient cells (left) and EVs (right) in the DESeq2 analysis in (C) and (E). (G) Gene expression comparison between EVs secreted by LCH patients with non-active or active disease. Red dots in (C), (E) and (G) are genes with significantly different expression.

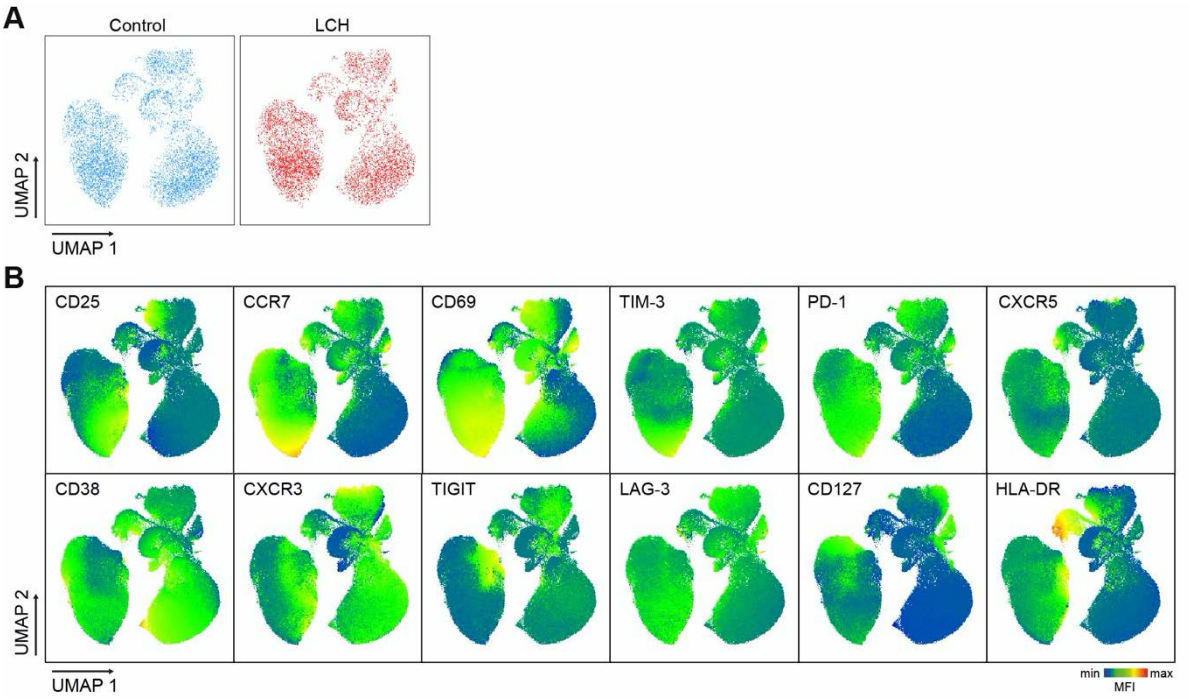

Figure S8: UMAP of lymphocytes treated with supernatants from control or LCH cultures. (A) UMAP on concatenated files of 114000 lymphocytes from 3 healthy donors (38000 cells from each donor) treated with control culture supernatant (light blue) or 114000 lymphocytes from the same 3 healthy donors (38000 cells from each donor) treated with LCH culture supernatant (red). (B) Combined UMAP of control-treated and LCH-treated lymphocytes displaying the median fluorescence intensity (MFI) of the indicated markers.

Supplemental references

1. Bost JP, Saher O, Hagey D*, et al.* Growth Media Conditions Influence the Secretion Route and Release Levels of Engineered Extracellular Vesicles. Adv Healthc Mater.2022;11:e2101658.

2. Hagey DW, Kordes M, Gorgens A*, et al.* Extracellular vesicles are the primary source of blood-borne tumour-derived mutant KRAS DNA early in pancreatic cancer. J Extracell Vesicles.2021;10:e12142.

3. Picelli S, Bjorklund AK, Faridani OR*, et al.* Smart-seq2 for sensitive full-length transcriptome profiling in single cells. Nat Methods.2013;10:1096-8.

4. Love MI, Huber W, Anders S. Moderated estimation of fold change and dispersion for RNA-seq data with DESeq2. Genome Biol.2014;15:550.

5. Hagey DW, Topcic D, Kee N*, et al.* CYCLIN-B1/2 and -D1 act in opposition to coordinate cortical progenitor self-renewal and lineage commitment. Nat Commun.2020;11:2898.

6. Johnson WE, Li C, Rabinovic A. Adjusting batch effects in microarray expression data using empirical Bayes methods. Biostatistics.2007;8:118-27.

7. Hagey DW, Zaouter C, Combeau G*, et al.* Distinct transcription factor complexes act on a permissive chromatin landscape to establish regionalized gene expression in CNS stem cells. Genome Res.2016;26:908-17.

8. Halbritter F, Farlik M, Schwentner R*, et al.* Epigenomics and Single-Cell Sequencing Define a Developmental Hierarchy in Langerhans Cell Histiocytosis. Cancer Discov.2019;9:1406-21.

9. Stuart T, Butler A, Hoffman P*, et al.* Comprehensive Integration of Single-Cell Data. Cell.2019;177:1888-902 e21.

10. Javadi J, Gorgens A, Vanky H*, et al.* Diagnostic and Prognostic Utility of the Extracellular Vesicles Subpopulations Present in Pleural Effusion. Biomolecules.2021;11:1606.

11. Wiklander OPB, Bostancioglu RB, Welsh JA*, et al.* Systematic Methodological Evaluation of a Multiplex Bead-Based Flow Cytometry Assay for Detection of Extracellular Vesicle Surface Signatures. Front Immunol.2018;9:1326.

12. Lourda M, Olsson-Akefeldt S, Gavhed D*, et al.* Detection of IL-17A-producing peripheral blood monocytes in Langerhans cell histiocytosis patients. Clin Immunol.2014;153:112-22.

13. Lourda M, Dzidic M, Hertwig L*, et al.* High-dimensional profiling reveals phenotypic heterogeneity and disease-specific alterations of granulocytes in COVID-19. Proc Natl Acad Sci U S A.2021;118:

14. Allen CE, Li L, Peters TL*, et al.* Cell-specific gene expression in Langerhans cell histiocytosis lesions reveals a distinct profile compared with epidermal Langerhans cells. J Immunol.2010;184:4557-67.